RSC Applied Polymers

ROYAL SOCIETY OF CHEMISTRY

PAPER

View Article Online
View Journal

Cite this: DOI: 10.1039/d5lp00399g

Polyethylene (PE) vitrimer by cross-linking two mass-produced ethylene-based polymers through one-step reactive blending

Xuanwei Zhang,[a] Siyu Guo,[a] Xiaopei Li[b] and Yongjie Zhang*[a]

Cross-linked polyethylene (XLPE) possesses excellent performance, making it an ideal choice for diverse applications. Yet traditional XLPE is hard to reprocess and recycle due to its three-dimensional cross-linked networks, causing serious environmental issues. Vitrimers, which combine the advantages of thermoplastics and thermosets, offer promising solutions for reuse of post-consumed XLPE. Although significant advances have been achieved, the preparation of polyethylene (PE) vitrimers in scalable, cost-effective, and efficient manners still remains a huge challenge. Here, we propose an industry-inspired strategy to obtain cost-effective PE vitrimers by directly cross-linking two mass-produced commodity ethylene-based polymers. Through a one-step reactive blending approach, trimethoxysilane-grafted polyethylene (TMS-PE) and ethylene vinyl acetate copolymer (EVA) were cross-linked *via* efficient transesterification between carboxylates and silicates, generating PE vitrimers with dynamic silicate (Si–O–C) cross-linkages. During the reactive blending process, considerable increases in torque were observed due to increases in viscosities after cross-linking, providing a solid proof for the successful preparation of targeted PE vitrimers. The transesterification was validated *via* the consumption of ester groups in EVA as revealed by FTIR analysis. The successful construction of robust cross-linked PE networks was further systematically analyzed by gel fraction testing and dynamic mechanical analysis (DMA). The thermomechanical and tensile properties of resultant vitrimers could be readily fine-tuned by simply adjusting the feed ratios. Compared to the pristine EVA, the tensile strength and Young's modulus of the vitrimers nearly doubled and increased by eight times, respectively. The tensile strength, Young's modulus, and elongation at break of PE vitrimers were well maintained after two reprocessing cycles, demonstrating their excellent recyclability. In summary, this work provides a practical solution for the preparation of low-cost and high-performance PE vitrimers, paving the way to the widespread and up-scaled use of recyclable XLPE.

Received 15th December 2025,
Accepted 6th April 2026

DOI: 10.1039/d5lp00399g

rsc.li/rscapplpolym

1 Introduction

The cross-linked structure imparts XLPE with excellent thermal resistance, high chemical inertness, high electrical insulation, and robust mechanical properties,[1,2] making it widely applied in critical fields such as cable insulation, heat-shrinking pipes, and storage tanks. XLPE accounts for 5–10% of total PE, sharing a comparable global market scale with polystyrene and polyethylene terephthalate.[3] XLPE is typically prepared by three traditional methods, including peroxide cross-linking,[4,5] irradiation cross-linking,[6,7] and silane cross-linking (Scheme 1a).[8,9] Peroxide and irradiation cross-linking form stable C–C cross-linkages, while silane cross-linking forms Si–O–Si cross-linkages. Owing to the stable cross-linking networks, traditional XLPE is hard to recycle or reprocess post-service, leading to significant resource waste and environmental pollution. There exists an urgent need to develop low-cost and high-performance recyclable XLPE.[10,11]

Advancements in vitrimers have blurred the line between thermosets and thermoplastics, offering new opportunities for the recycling and reuse of traditional cross-linked polymers.[12–16] Vitrimers are defined as permanent networks of polymers cross-linked by dynamic bonds.[14] The associative dynamic bond exchange renders the network topology to undergo rearrangement while maintaining the chemical integrity of the polymer network.[17] Featured by excellent performance and easy reprocessing, vitrimers have aroused wide interest in both academia and industry. Various dynamic covalent bonds, such as ester exchange,[18–20] alkyl exchange,[21,22] boronic ester exchange,[23–25] disulfide exchange,[26–28] and imine exchange,[29–31] have been introduced into cross-linked polymers to develop diverse vitrimers. Specifically, extensive

[a]School of Textile and Material Engineering, Dalian Polytechnic University, Dalian 116034, China
[b]Instrumental Analysis Centre, Dalian Polytechnic University, Dalian 116034, China

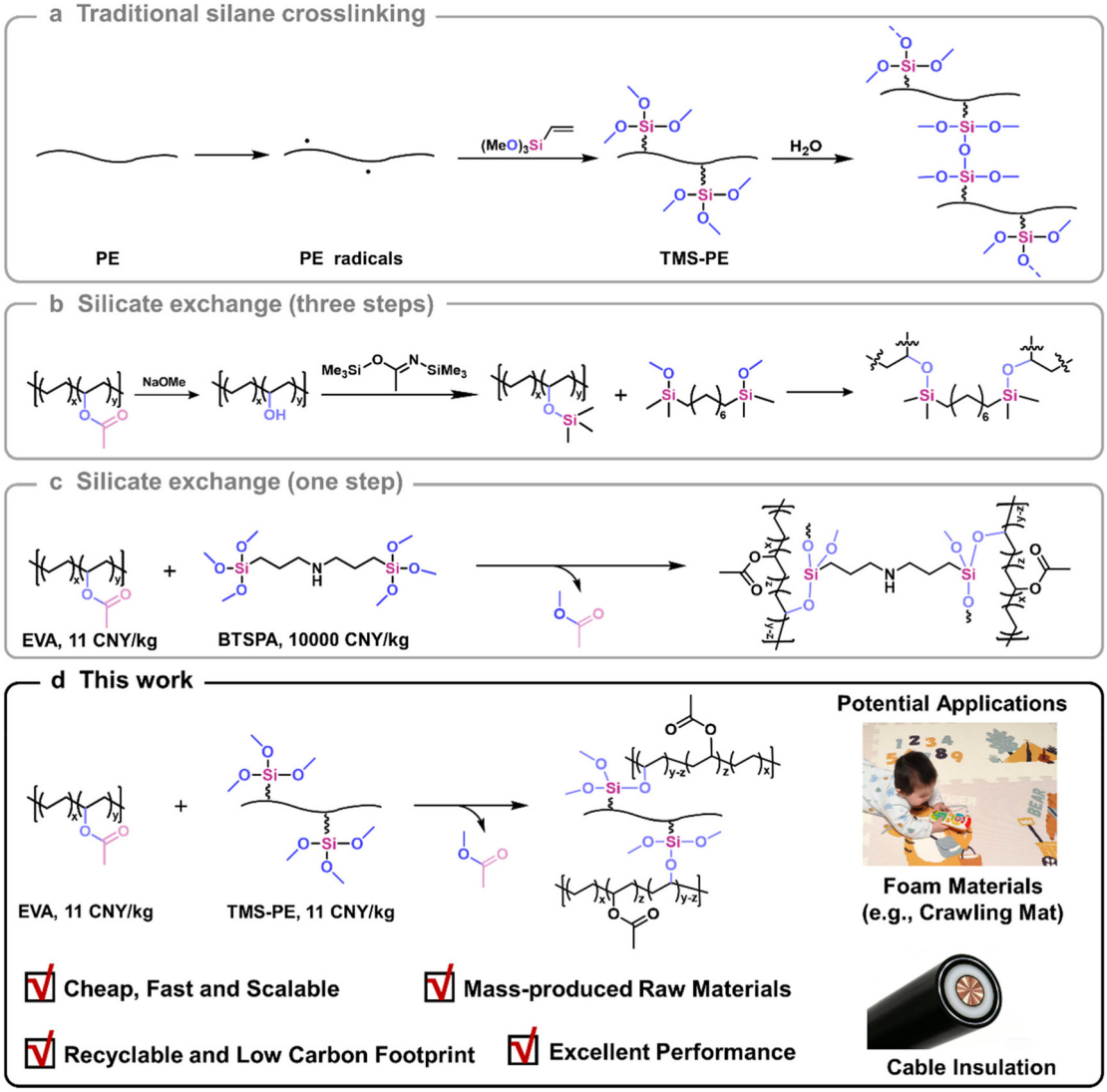

Scheme 1 Comparisons of strategies for XLPE: (a) traditional XLPE *via* silane cross-linking; (b) silicate-based PE vitrimer *via* three-step synthesis; (c) silicate-based PE vitrimer *via* one-step synthesis starting from an expensive cross-linker; (d) silicate-based PE vitrimer *via* one-step synthesis with two mass-produced ethylene-based polymers as precursors.

attention has been drawn to polyolefin vitrimers due to the huge demand for recyclable cross-linked polyolefins.

There are mainly three strategies to prepare polyolefin vitrimers: (1) cross-linking commodity polyolefins with difunctional cross-linkers containing dynamic covalent bonds;[32] (2) cross-linking functionalized polyolefins obtained by copolymerization of olefin and polar monomers;[33,34] (3) cross-linking commercial reactive polyolefins.[35,36] The former two approaches often involve tedious synthetic processes and expensive raw materials, limiting their applications in developing cost-effective polyolefin vitrimers. Directly cross-linking abundant commercial reactive polyolefins represents a straightforward and practical route for preparing high-performance polyolefin vitrimers. Those polyolefins include maleic anhydride-grafted polyethylene (MA-*g*-PE), maleic anhydride-grafted polypropylene (MA-*g*-PP), glycidyl methacrylate-grafted polyethylene (GMA-*g*-PE), ethylene-acrylic acid copolymer (EAA), and ethylene–vinyl acetate copolymer (EVA).[37–41] Ouyang *et al.*[42] developed polyolefin vitrimers through utilization of the carboxyl groups generated by hydrolysis of MA-*g*-PP and the epoxy groups in GMA-*g*-PE, which were then blended with the resultant product with low-density polyethylene to generate thermoplastic cable insulation material. The resultant insulation material exhibited good thermomechanical and electrical properties. Li *et al.*[43] demonstrated that PE vitrimers generated by reacting MA-*g*-PE with epoxy resin possessed outstanding electrical properties, such as high energy storage and electrical damage self-healability. Zhang *et al.*[44] prepared a novel PE vitrimer by reactive blending MA-*g*-PE with trimethylolpropane tris(3-mercaptopropionate), forming dynamic thioester bonds *via* a condensation reaction between anhydride and thiol. The developed PE vitrimers exhibited

excellent insulation properties and reprocessability. Notably, ethylene–vinyl acetate copolymer (EVA) can undergo a special ester exchange reaction with borate, leading to B–O–C covalent bond cross-linked EVA vitrimers.[40,45] The dynamic cross-linking network allowed for self-healing of processing damage and multiple recycling *via* B–O–C rearrangement.[45] Similarly, Guan *et al.*[46] prepared EVA vitrimers (Scheme 1b) with superior mechanical and thermal properties *via* transesterification between bis(methoxydimethyl)silyl octane and trimethylsilyl ether functional polymer, a silylated ethylene–vinyl alcohol copolymer (hydrolyzed EVA). However, the process requires tedious synthetic steps, limiting its potential applications. Inspired by these studies, we developed a novel one-step and scalable approach to prepare EVA vitrimers, taking advantage of transesterification between carboxylic esters in EVA and silicic esters in bis[3-(trimethoxysilyl)propyl]amine, representing a promising way for large-scale production of EVA vitrimers (Scheme 1c).[47] Nevertheless, due to the high cost of reagent-grade cross-linker, EVA vitrimers produced by this approach are still not affordable for general applications.

Silane cross-linking technology is a widely used industrial process to produce XLPE with enhanced thermodimensional stability. This technology includes two steps: (1) peroxide-activated grafting of silane onto the PE backbone to obtain alkoxysilane-grafted PE (usually TMS-PE), (2) cross-linking through condensation of side-grafted alkoxysilanes in a water bath or steam chamber (Scheme 1a).[48] TMS-PE is a mass-produced, highly reactive functionalized PE with a low cost (around 11 CNY per kg). Inspired by the factors mentioned above, we propose that the transesterification between silicate in TMS-PE and carboxylate in EVA could be utilized to construct PE vitrimers cross-linked by dynamic Si–O–C bonds (Scheme 1d). Featured by its straightforward preparation approach, abundant raw materials, and outstanding performances, the strategy demonstrated herein represents a sustainable and business-appealing method for recyclable polyolefins. The vitrimer reported herein can be mass-produced with existing industrial equipment at a cost comparable to that of commercial cross-linked EVA and silane-cross-linked polyethylene, positioning it as a promising alternative in applications such as foaming materials and cables. Its excellent reprocessability also offers potential to reduce the carbon footprint and advance sustainability in the XLPE industry.

2 Experimental sections

2.1 Materials

Tetrabutyl titanate (TT-01, ≥99%, Beijing InnoChem Science and Technology Co., Ltd), xylene (≥99%, Tianjin Kemiou Chemical Reagent Co., Ltd), and antioxidant (AO225, Linyi Sanfeng Chemical) were used as received. Ethylene-vinyl acetate copolymer (EVA, UE2825; MFI = 25.4 g per 10 min) containing 28 wt% vinyl acetate was sourced from Jiangsu Sierbang Petrochemical Co., Ltd, whereas the TMS-PE (code: 101A; graft ratio of vinylsilane: 1 wt%; density: 0.92 g cm^{-3}) was obtained from Zhejiang Wanma Macromolecule Co., Ltd. All the chemicals were used as-received without further purification.

2.2 Preparation of vitrimers

PE vitrimers were synthesized *via* reactive blending. EVA (20 g, 100 phr, ester group = 65.2 mmol), antioxidant AO225 (0.1 g), TT-01, and TMS-PE were loaded into a torque rheometer (Model RTOI-06/02, Guangzhou Potop Experimental Analytical Instrument Co., Ltd) and mixed at 170 °C for 20 minutes. The addition amounts of TMS-PE were 60 phr, 90 phr, and 120 phr, respectively, and the resulting PE vitrimers from the cross-linking reaction were named Si60, Si90, and Si120. The cross-linking density of PE vitrimers were controlled by adjusting the amount of TMS-PE under the conditions that the ester groups are in excess relative to trimethoxysilane groups. The estimated amounts of trimethoxysilane groups for 60, 90, and 120 phr TMS-PE are 2.4, 3.6, and 4.8 mmol. The resultant mixture was compression-molded in a plate vulcanizing press machine (Model YT-LH 102A, Dongguan Yitong Testing Technology Co., Ltd) at 210 °C and 10 MPa for 20 minutes.

2.3 Gel fraction

The cured material was cut to an appropriate weight (around 100 mg; $m_{original}$) and placed in a two-neck flask with 50 mL of xylene. The sample was then immersed at 120 °C for 16 hours to allow for swelling. After swelling, the material was placed in a vacuum oven and heated to 100 °C, followed by vacuum drying for 12 hours. The residual solvent was removed, and the material was weighed ($m_{ultimate}$), and the gel fraction was calculated using the eqn (1):

$$\text{Gel fraction} = \frac{m_{ultimate}}{m_{original}} \times 100\%. \quad (1)$$

2.4 Characterizations

Field emission scanning electron microscopy (SEM) was performed using a JSM-7800F microscope (JEOL Ltd, Japan) to observe the surface micro-morphology of the PE vitrimers, which were freeze-fractured after immersion in liquid nitrogen. Elemental mapping of silicon was conducted using an X-Max50 energy dispersive X-ray spectrometer (EDS) (Oxford Instruments, UK) attached to the same SEM instrument. Attenuated total reflectance Fourier transform infrared (ATR-FTIR) spectra were recorded on a Spectrum Two FT-IR Spectrometer (PerkinElmer, USA) with a spectral resolution of 4 cm^{-1}, covering a wavenumber range of 4000 to 500 cm^{-1}. Differential scanning calorimetry (DSC) was performed using a DSC Q2000 instrument (TA Instruments, USA) under a nitrogen atmosphere with a flow rate of 50 mL min^{-1}. The measurements followed a heat-cool-heat cycle at a rate of 10 °C min^{-1}. The melting temperature (T_m) was determined from the second heating scan. Thermogravimetric analysis (TGA) was carried out using a TGA-2 (Mettler Toledo, Switzerland), with a temperature ramp from 30 °C to 650 °C at 10 °C min^{-1} under a nitrogen atmosphere. Isothermal weight loss measurements

were performed under nitrogen at 210 °C for 60 minutes. Dynamic mechanical thermal analysis (DMTA), creep, and stress relaxation tests were performed on a DMA Q800 analyzer (TA Instruments, USA) using rectangular specimens (30 mm × 6 mm × 1 mm). DMTA temperature sweeps were conducted from 30 to 200 °C at a heating rate of 3 °C min^{-1}, with a frequency of 5 Hz and an amplitude of 15 μm. The creep test applied a stress of 0.05 MPa for 30 minutes, followed by unloading and recovery for 30 minutes. For stress relaxation tests, the specimens were mounted in tensile mode, subjected to a constant strain of 6%, and the resulting stress decay was monitored over time. Tensile tests were performed using a universal testing machine (AGX-10KN, Shimadzu, Japan) at a deformation rate of 10 mm min^{-1} with dimensions of 2 mm × 1 mm × 20 mm. The average mechanical properties and standard deviation were calculated. For recyclability evaluation, the samples were recycled, crushed, and reprocessed at 210 °C and 10 MPa for 20 minutes before repeating the tensile test.

3 Results and discussion

3.1 Torque rheometer curves

The torque rheometer curves were utilized to monitor the cross-linking reaction of EVA and TMS-PE in the internal mixer (Scheme 2a). As shown in Fig. 1A, the torque of parent EVA rapidly reached a peak at 20 s, followed by a sharp decline to a lower plateau corresponding to the melting process of EVA. For the EVA/TMS-PE mixtures, after the melting process, the torques increased rapidly at around 75 s, indicating the onset of cross-linking through the transesterification between silicate in TMS-PE and carboxylate in EVA. Subsequently, the torque gradually decreased and eventually stabilized at an equilibrium value around 800 s, remaining stable thereafter. At this point, the cross-linking reaction was considered to be nearly complete. Therefore, torque rheometer curves provided the first proof for the successful preparation of targeted PE vitrimers. Moreover, the plateau torques of Si60 (~9.4 N m), Si90 (~20.0 N m), and Si120 (~23.9 N m) increased as the proportion of TMS-PE, indicating the cross-linking density of PE vitrimers could be fine-tuned by adjusting EVA/TMS dosages.[49]

To further substantiate the cross-linking reaction process, the micro-morphologies of PE virtrimers were studied using SEM and SEM-EDS (Fig. S1). Although the report by Faker *et al.* showed that PE/EVA blends with comparable proportions of PE and EVA exhibit co-continuous phases,[50] no obvious phase separation was observed for PE vitrimers composed of EVA and TMS-PE segments. Silicon element mapping images also revealed a uniform distribution of silicon in the PE vitrimers. The good compatibility between EVA and TMS-PE in the PE vitrimers can be attributed to the following two factors. First, TMS-PE with polar siloxane side groups is more compatible with EVA compared to nonpolar PE. Second, the cross-linking reaction between TMS-PE and EVA can form a "graft copolymer" (*i.e.*, EVA-*graft*-TMS-PE), acting as a compatibilizer to further enhance their compatibility. The proposed cross-linking process is as follows. Initially, the polarity of TMS-PE promotes its compatibility with EVA, ensuring that TMS-PE and EVA are uniformly mixed and undergo transesterification reactions. Subsequently, the resultant graft copolymer of TMS-PE and EVA acts as a compatibilizer, further enhancing their compatibility.[51–53] Ultimately, the macromolecular chains of TMS-PE and EVA interpenetrate and entangle with each other, forming a three-dimensional cross-linked network to yield the target product PE vitrimers.

3.2 FTIR analysis and gel fraction test

The chemical structures of PE vitrimers and pristine EVA were characterized by FTIR spectroscopy (Fig. 1B). The absorption peaks at 2920 and 2850 cm^{-1} correspond to the asymmetric and symmetric stretching vibrations of C–H bonds, while the absorption peak at 1740 cm^{-1} corresponds to the stretching vibration of the ester carbonyl group (C═O). Compared to EVA, the characteristic peak at 1740 cm^{-1} decreased significantly with increasing TMS-PE dosage for Si60, Si90, and Si120. As shown in Fig. 1C and Table S1, the consumption of ester groups (13.9% to 27.6%) (eqn (S1)) and the gel fractionts of PE vitrimers (37.7 wt% to 60.9 wt%) both steadily increased with TMS-PE dosage, reaffirming that the cross-linking degrees of PE vitrimers could be easily tailored by selecting feeding ratios.

Considering the potential self-cross-linking of TMS-PE, TMS-PE was first mixed in a torque rheometer and molded into a sheet following the same protocol as that used for the PE vitrimers. The measured gel fraction of self-cross-linked TMS-PE was 46.6 wt%. According to the feeding ratios of TMS-PE and EVA, the calculated maximum contributions of TMS-PE self-cross-linking to the total gel fraction are 17.5 wt%, 22.1 wt%, and 25.4 wt% for Si60, Si90, and Si120, respectively, which are substantially lower than the measured gel fractions. Furthermore, the cross-linking reaction between EVA and TMS-PE is expected to further suppress the self-cross-linking of TMS-PE. Therefore, it is reasonable to speculate that the cross-linking reaction between EVA and TMS-PE is the dominant process in network formation.

3.3 Thermal and thermal mechanical properties of PE vitrimers

DSC analyses revealed that two sets of separated melting peaks (~67 °C for EVA and ~110 °C for TMS-PE) were observed for PE vitrimers, indicating that even after cross-linking, EVA and TMS-PE both have their own crystallization processes. The melting points (T_m) of cross-linked EVA and TMS-PE in PE vitrimers both monotonicity decreased as the cross-linking degree increased. A similar trend was observed for the melting enthalpy, crystallization enthalpy, and crystallinity of cross-linked EVA in PE vitrimers (Table 1 and Table S2). Moreover, the melting enthalpy, crystallization enthalpy, and crystallinity of cross-linked TMS-PE also considerably decreased compared to those of parent TMS-PE. These findings indicated that the crystallization processes of EVA and TMS-PE were hindered

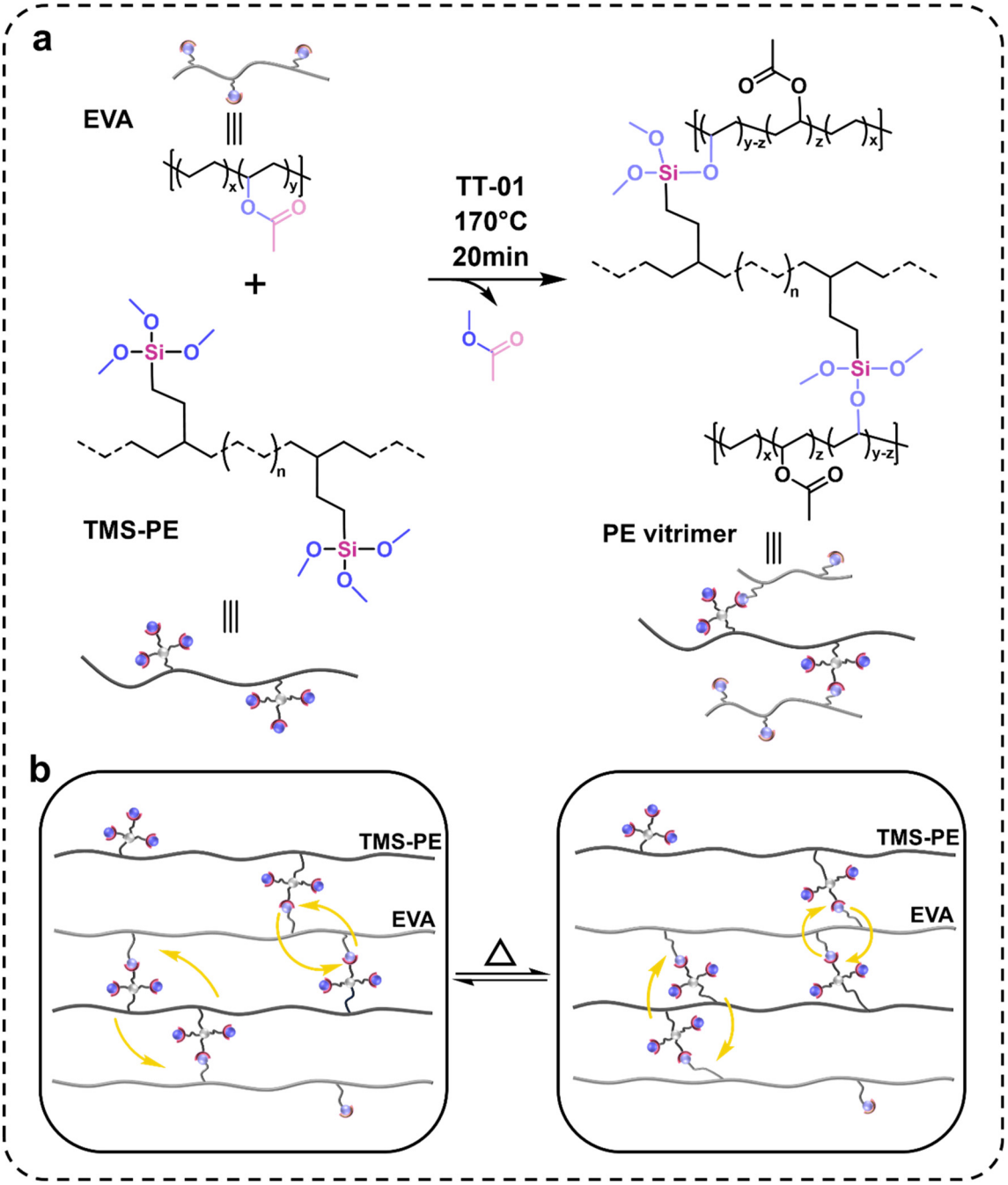

Scheme 2 (a) PE vitrimers with dynamic Si–O–C cross-linkage prepared *via* the transesterification between silicate in TMS-PE and carboxylate in EVA, and (b) network topological rearrangement of PE vitrimers achieved *via* dynamic transesterification.

upon cross-linking owing to the restricted mobility of macromolecular chains.[47,54,55]

TGA was performed to evaluate the thermal stability of PE vitrimers. Fig. S2 compares the TGA curves of the raw materials and the PE vitrimers over a temperature range of 50 °C to 600 °C under a N_2 atmosphere, with the corresponding data summarized in Table 1. The initial decomposition temperatures of Si60, Si90, and Si120 were all above 339 °C, which is higher than that of EVA (330.20 °C) but lower than that of TMS-PE (436.20 °C). The initial decomposition temperature of the PE vitrimers increased consistently with cross-linking density. The relationship between the initial decomposition temperature of the materials and the TMS-PE content is shown in Fig. S3. The initial decomposition temperature exhibited a quasi-exponential correlation with TMS-PE. Our prior research on EVA vitrimers based on dynamic silicate and titanate bonds demonstrated that their thermal stability is not significantly influenced by cross-linking degree.[47,56] Given

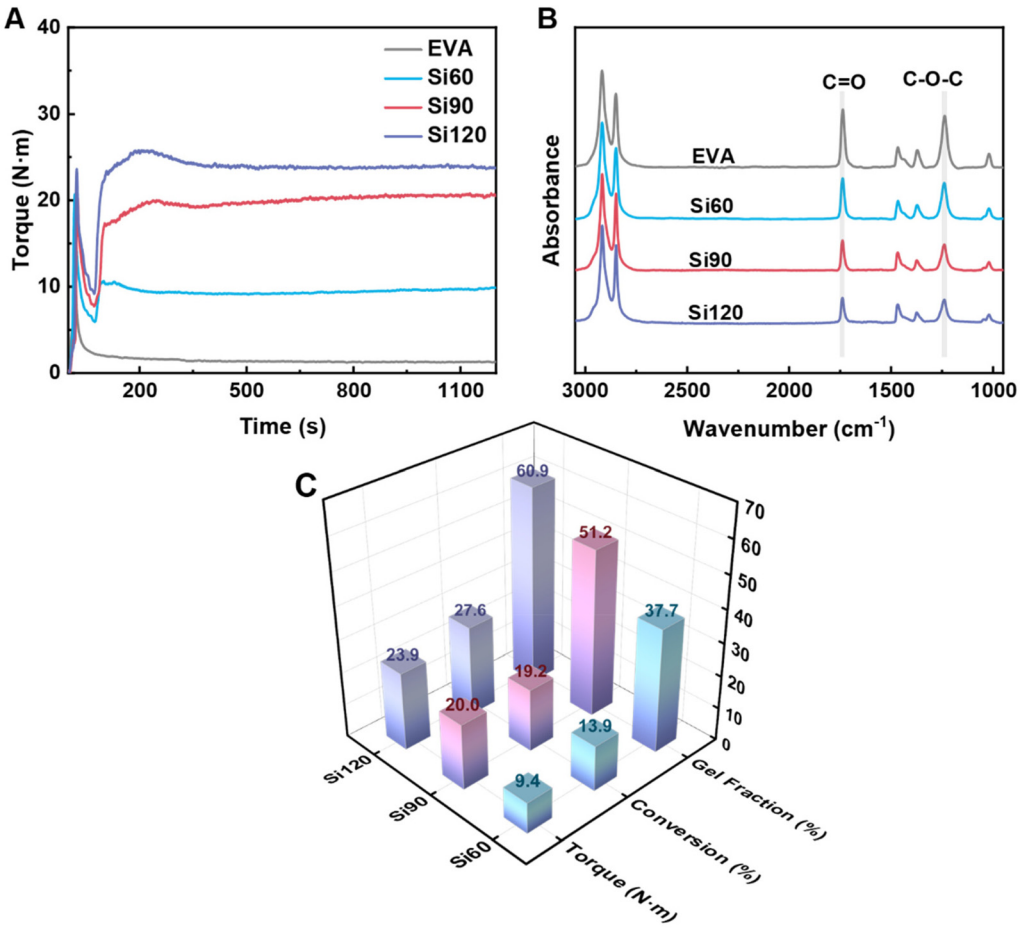

Fig. 1 (A) Typical torque curves of parent EVA and PE vitrimers; (B) FTIR spectra of parent EVA and PE vitrimers, and (C) 3D visualization of torque, ester conversion, and gel fraction evolution in PE vitrimers.

Table 1 Thermal properties of raw materials and PE vitrimers

Sample	$T_{m,\ EVA}$ [a] (°C)	$T_{m,\ TMS\text{-}PE}$ [b] (°C)	$\Delta H_{m,\ EVA}$ [a] (J g^{-1})	$\Delta H_{m,\ TMS\text{-}PE}$ [b] (J g^{-1})	$X_{c,\ EVA}$ [a] (%)	$X_{c,\ TMS\text{-}PE}$ [b] (%)	$T_{d5\%}$ (°C)	w [c] (wt%)
EVA	73.88	—	29.24	—	9.98	—	330.20	—
TMS-PE	—	121.57	—	58.50	—	20.09	436.20	—
Si60	69.65	112.50	19.81	46.32	6.76	15.81	339.84	0.41
Si90	67.30	111.81	18.02	49.49	6.15	16.89	342.67	0.33
Si120	65.07	111.88	14.53	49.56	4.96	16.91	346.90	0.46

[a] Normalized to EVA for PE vitrimers. [b] Normalized to TMS-PE for PE vitrimers. [c] Weight losses of vitrimers at 60 minutes in isothermal TGA tests.

that the PE vitrimers reported herein possess a cross-linked structure analogous to the previous EVA vitrimers, it is reasonable to infer that their thermal stability is relatively insensitive to its crosslinking degree. TGA results indicate a significantly higher onset decomposition temperature for TMS-PE compared to EVA, attributed to the abundance of ester groups that are susceptible to thermal degradation. Increasing the TMS-PE content concurrently enhances both the cross-linking density and the proportion of TMS-PE. Therefore, it can be concluded that the improvement in the onset decomposition temperature of the PE vitrimers is primarily due to the increased proportion of TMS-PE. The weight losses of all PE vitrimer were found to be negligible (<0.5 wt%), after heating at 210 °C for 60 minutes, as revealed by the isothermal weight loss curves (Fig. 2B). This indicates that the materials can be reprocessed and reshaped without significant degradation at this temperature.

The thermomechanical properties of PE vitrimers, pristine EVA, and TMS-PE were investigated using DMTA. As shown in Fig. 3, the storage modulus of pristine EVA decreased sharply

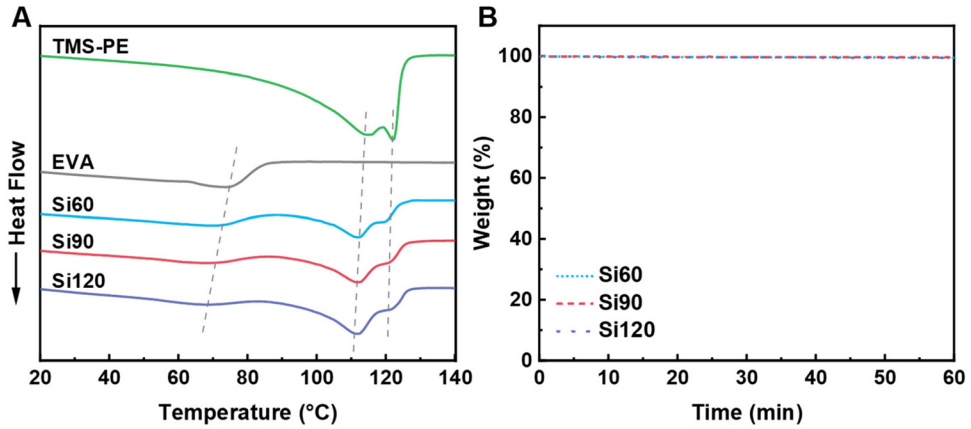

Fig. 2 (A) DSC curves of endothermic peaks for the PE vitrimers and raw materials; (B) isothermal TGA curves of Si60, Si90, and Si120 at 210 °C (N_2 atmosphere).

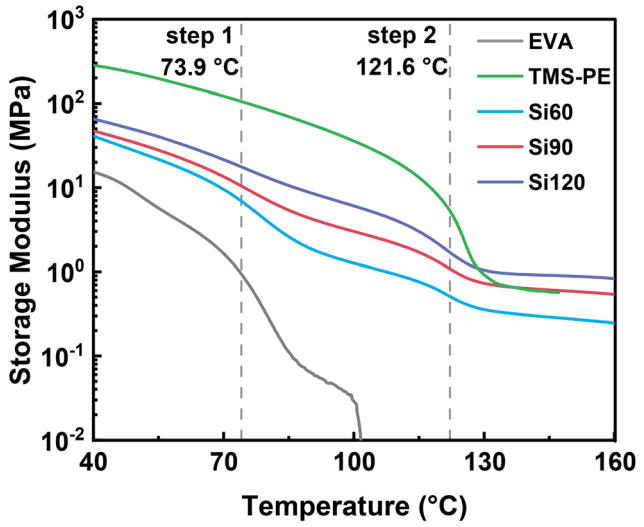

Fig. 3 DMTA profiles of the PE vitrimers and their precursors.

with increasing temperature, dropping to nearly zero at 101.9 °C, corresponding to the melting processes of EVA. As the temperature increased, the storage moduli of PE vitrimers exhibited an overall gradual decline, interrupted by two distinct, abrupt downward steps. Step 1 and step 2 corresponded to the melting processes of EVA and TMS-PE, respectively, indicating that the EVA and TMS-PE segments in PE vitrimers may independently crystallize to form separated EVA and TMS-PE crystallites. The crystalline phases of EVA and TMS-PE act as physical cross-linking sites to keep the materials with high moduli,[57] which witnessed sharp decreases when the crystalline phases were destroyed by melting at around 73.9 °C and 121.6 °C. Step 2 was more pronounced with increased dosages of TMS-PE, and *vice versa*. Due to covalent cross-linking, the molten PE vitrimer network retains its mechanical strength, displaying a distinct rubbery plateau—a characteristic feature of cross-linked systems.[34,58] According to the molecular theory of rubber elasticity, the modulus of the rubbery plateau is directly proportional to the cross-linking density,[59] meaning that a higher plateau height corresponds to a higher cross-linking density. At 134 °C, the rubbery plateau moduli of Si60, Si90, and Si120 increased with the degree of cross-linking obtained from gel fraction testing, with measured values of 0.33 MPa, 0.68 MPa, and 0.97 MPa, respectively. From these values, the average molecular weights of Si60, Si90, and Si120 between cross-links (M_c) were calculated to be 27.7, 13.5, and 9.4 kg mol^{-1}, respectively, meaning that the cross-linking networks could be readily controlled by adjusting the weight ratio of EVA to TMS-PE (Table S3, eqn (S2)). It is worthy to point out that the DMTA profile of pure TMS-PE also showed a characteristic rubbery plateau at elevated temperatures, probably due to the self-cross-linking of highly reactive side-grafted methoxysilane groups in TMS-PE during the molding process.

3.4 Stress relaxation behavior and creep resistance

Under a constant strain of 6% in linear viscoelastic conditions, the dynamics of topology network rearrangement due to the Si–O–C bond exchange reaction were evaluated through typical stress relaxation experiments conducted at elevated temperatures. The obtained stress relaxation curves were first fitted to Maxwell (eqn (2)) and Kohlrausch–Williams–Watts (KWW, eqn (3)) models.[60–62] Yet significant differences were observed between the experimental data and the fitted curves obtained using the Maxwell (Fig. 4A) and KWW (Fig. 4B) models. Then, binary KWW model (eqn (4)) was selected, which assumes two relaxation processes, fast and slow, coexist. It turned out that the experimental data showed good agreement with the fitted curve of the binary KWW model.[63] The fast and relaxation models are considered to be driven by bond exchange reaction and diffusion (involving chain entanglement, segmental motion, *etc.*), respectively.[64]

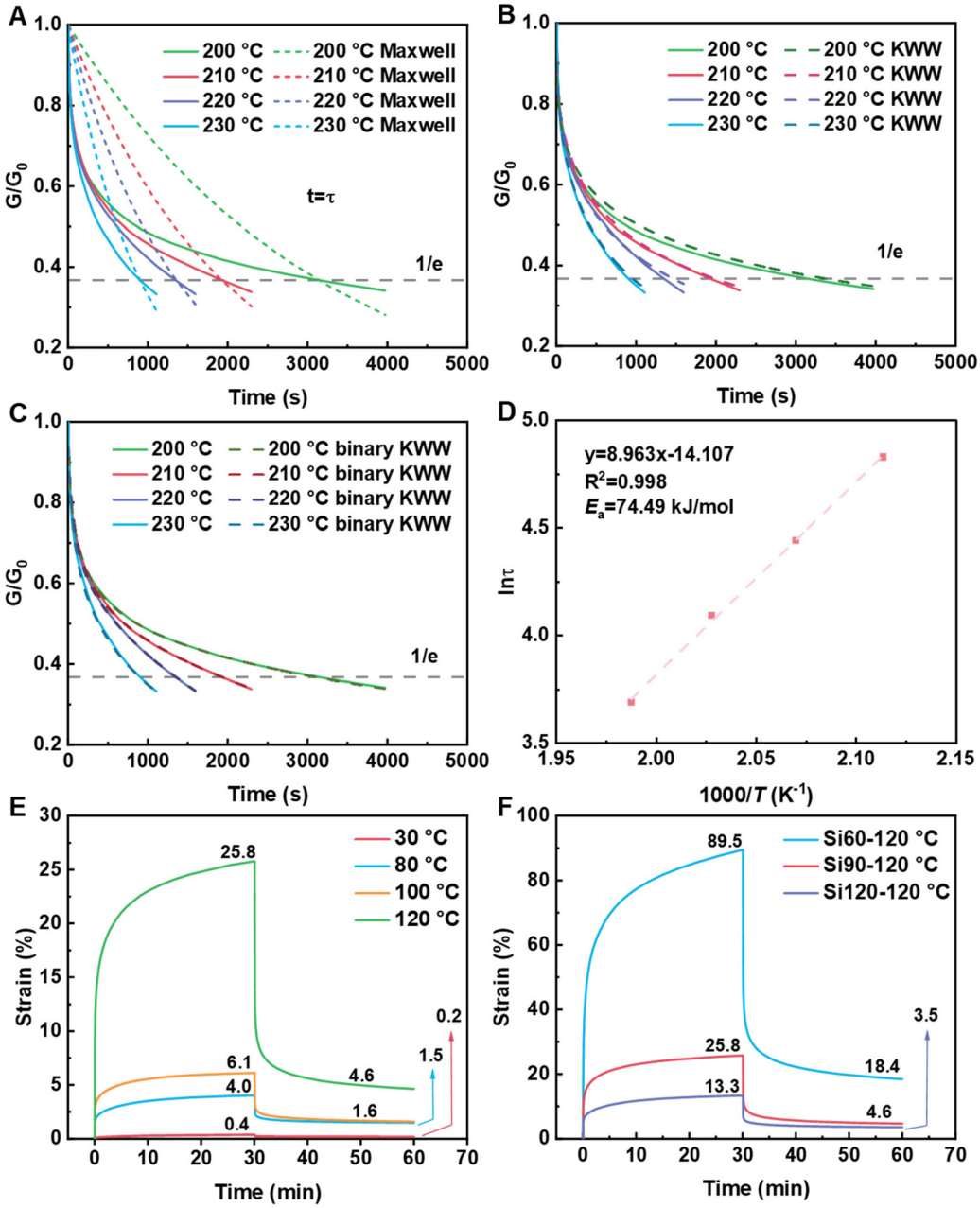

Fig. 4 (A) Comparison between stress relaxation curves and Maxwell model curves (solid: original stress relaxation data of Si90 at various temperatures; dashed: Maxwell curves, where the τ^* values were the same as τ^* values determined by the original stress relaxation curves at given temperatures); (B) comparison between stress relaxation curves and KWW model curves (dashed: KWW fitted curves); (C) comparison between stress relaxation curves and binary KWW model curves (dashed: binary KWW fitted curves); (D) linear fitting of ln(τ) *vs.* 1000/T for determining the activation energy of stress relaxation; (E) creep curves of Si90 measured at different temperatures with a constant stress of 0.05 MPa; (F) creep curves of Si60, Si90, and Si120 measured at 120 °C.

$$G = G_0 \times \exp\left(-\frac{\tau^*}{t}\right) \quad (2)$$

$$\frac{\sigma(t)}{\sigma_0} = \exp\left(-\frac{t}{\tau}\right)^{\beta} \quad (3)$$

where τ is the specific relaxation time and β represents the distribution of τ.

$$\frac{\sigma(t)}{\sigma_0} = A_{\text{fast}} \exp\left\{-(t/\tau_{\text{fast}})^{\beta_{\text{fast}}}\right\} + A_{\text{slow}} \exp\left\{-(t/\tau_{\text{slow}})^{\beta_{\text{slow}}}\right\} \quad (4)$$

Curve fitting parameters obtained using eqn (4) were collected in Table 2. Accordingly, the τ_{fast} data in Table 2 were used to estimate the activation energy (E_a) of silicate exchange according to eqn (5).[65–69]

Table 2 Curve fitting parameters using eqn (4) for stress relaxation curves of Si90

Temperature (°C)	A_{fast}	τ_{fast} (s)	β_{fast}	A_{slow}	τ_{slow} (s)	β_{slow}
200	0.46	125	0.55	0.54	9900	0.81
210	0.35	95	0.61	0.65	4300	0.72
220	0.34	60	0.65	0.66	2450	0.90
230	0.18	40	0.95	0.82	1300	0.60

$$\tau^{\star} = \tau_0 \times \exp\left(\frac{E_a}{RT}\right) \quad (5)$$

Based on the relaxation time ($\tau^{\star}$) obtained from Fig. 4C, a master plot of $\ln(\tau)$ *versus* $1000/T$ was constructed and subsequently fitted with a linear regression line (Fig. 4D), where the slope corresponds to the activation energy divided by the gas constant. The activation energy of Si90 was calculated to be 74.5 kJ mol^{-1} (Fig. 4D), which falls within the previously reported range of 53–146 kJ mol^{-1} for silicate-based vitrimers.[46,47,70,71]

Permanent dynamic cross-linking can enhance the creep resistance of polymers and broaden their potential applications. The creep behaviors of precursor EVA and PE vitrimer were first compared at 65 °C. As shown in Fig. S4A, the stain of EVA after 1800 seconds was 41.0%, significantly higher than that of Si120 (0.3%). The excellent creep resistance of PE vitrimers could be explained by the restrictions on the movement of molecular chains after cross-linking, which thereby reduces deformation during loading. Subsequently, the creep behaviors of PE vitrimers were characterized through creep-recovery tests, where a constant stress of 0.05 MPa was applied for 1800 seconds, followed by stress removal and isothermal recovery. As depicted in Fig. 4E, the irrecoverable deformation of Si90 at 30 °C was merely 0.2%, much lower than that of linear EVA (Fig. S4B). The irrecoverable deformation was still as low as 1.5% at 80 °C, whereas linear EVA cannot be subjected to creep testing due to its molten state. Further enhancement in test temperatures resulted in an increase in irrecoverable deformation due to accelerated silicate exchange, yet the irrecoverable deformation observed at 120 °C was only 4.6%. At 80 °C (Fig. 4E), Si90 (1.5%) exhibits significantly improved resistance to deformation compared to recently reported EVA vitrimers (4.4%).[56]

Subsequently, the creep behaviors of PE vitrimers with different cross-linking densities were systematically studied at 120 °C (Fig. 4F). The strains of Si60, Si90, and Si120 after 1800 seconds of loading were 89.5%, 25.8%, and 13.3%, respectively, revealing that the creep resistance of PE vitrimers could be dramatically enhanced by increasing cross-linking density. Meanwhile, the final deformations of Si90 and Si120 (4.6% and 3.5%) after 3600 seconds were considerably lower than that of Si60 (18.4%), which reconfirmed that the creep resistance of PE vitrimers benefits from the higher cross-linking density. Increases in cross-linking density not only reduce the amount of free chains but also enhance the restrictions on the mobility of cross-linked chains through more cross-linking joints, both of which will lead to less chain migration and improved creep resistance.[47,72]

3.5 Mechanical properties and reprocessability

The mechanical properties of both the pristine EVA, self-cross-linked TMS-PE, PE vitrimers were evaluated through uniaxial tensile tests (Fig. 5A). Compared to the pristine EVA, the vitrimers exhibited significant enhancements in tensile strength and Young's modulus, accompanied by a reasonable reduction in elongation at break. Meanwhile, the tensile strengths and Young's modulus of PE vitrimers increased monotonously with their cross-linking densities. Specifically, the tensile strength and Young's modulus of Si120 with the highest cross-linking density increased by as high as 81.0% and 763.2%, respectively (Table 3). As expected, the elongation at breaks of PE vitrimers gradually decreased as the cross-linking densities increased, probably due to the restrictions of macromolecular chain movements. Meanwhile, the elongation at break of PE vitrimers was still as high as 665.64%–899.38%. Fig. 5B compared the mechanical properties of PE vitrimers and ethylene-based commodity polymers, which showed that the well-balanced mechanical properties of PE vitrimers were achieved (Table S4).

The reprocessability of the PE vitrimers was examined using Si90 as a representative sample. The initial Si90 material was crushed into particles and hot-pressed at 210 °C under a pressure of 10 MPa for two cycles. FTIR spectra of Si90 confirmed that no significant structural changes occurred before and after each reprocessing cycle (Table S5, Fig. S5). As illustrated in the stress–strain curves in Fig. 5C, even after two cycles of reprocessing, the material maintained its original mechanical properties, which were comparable to those of the initial Si90 (Table 3). Throughout the cycling process, the Young's modulus, tensile strength, elongation at break, and gel fraction of Si90 remained almost unchanged (Table 3, Fig. 5D), indicating excellent reprocessability and recyclability.

The tensile toughness (U) of the material was obtained by integrating the area under the stress–strain curve from the tensile test, as shown in eqn (6):[73]

$$U = \int_0^{\varepsilon} \sigma(\varepsilon) \mathrm{d}_{\varepsilon} \quad (6)$$

where U represents the tensile toughness, σ and ε denote stress and strain, respectively, and the unit of U is J cm^{-3}.

The results show that the tensile toughness of Si60 and Si120 were comparable to that of the raw EVA (71.15 ± 1.20 J cm^{-3}), while that of Si90 (76.98 ± 3.66 J cm^{-3}) was significantly improved. Apparently, tensile toughness is influenced by both elongation at break and tensile strength, which are often negatively correlated for most cross-linked polymers.[47,56] Therefore, the key to improving tensile toughness lies in striking a balance between these two factors. The above results indicate that Si90, with a moderate cross-linking degree, achieves an excellent balance between tensile strength and elongation at break, thus exhibiting the highest tensile toughness.

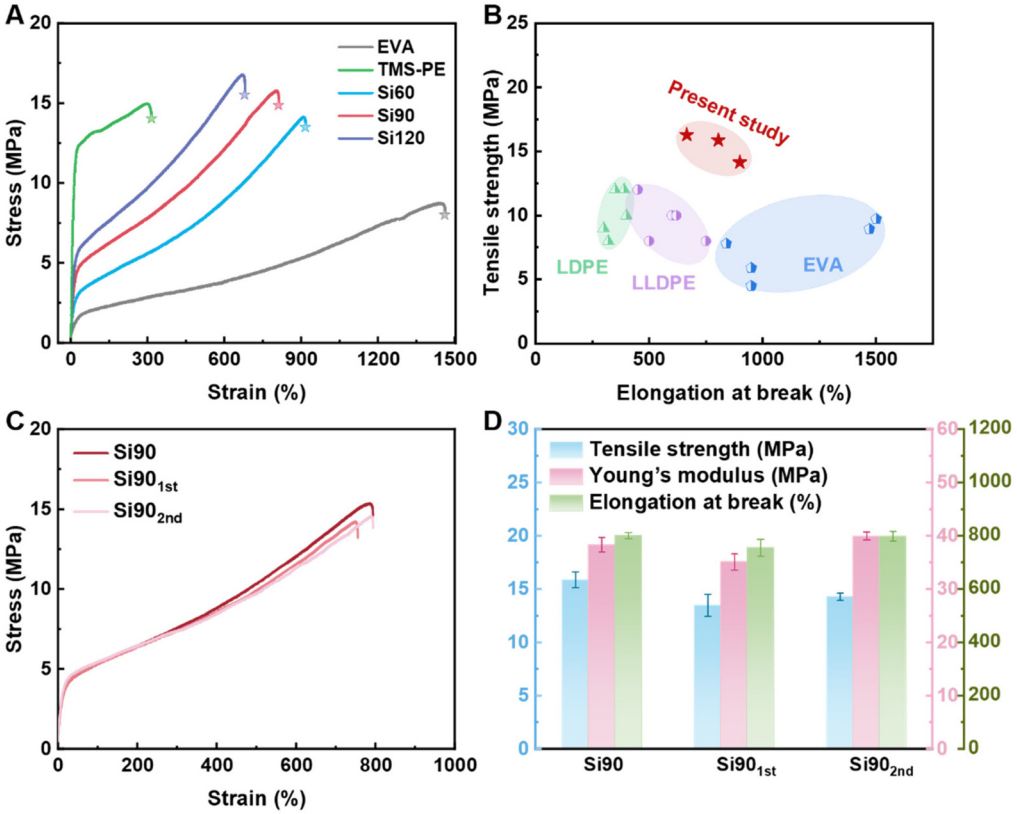

Fig. 5 (A) Stress–strain curves of the PE vitrimers, pristine EVA, and self-cross-linked TMS-PE (obtained by hot pressing under conditions identical to PE vitrimers); (B) comparison of mechanical properties of PE vitrimers and ethylene-based commodity polymers; (C) the representative stress–strain curves of the original Si90 and reprocessed Si90, and (D) mechanical properties of Si90 before and after reprocessing.

Table 3 Mechanical properties of parent EVA, self-cross-linked TMS-PE, PE vitrimers, and Si90 after reprocessing cycles

Sample	Tensile strength (MPa)	Young's modulus (MPa)	Elongation at break (%)	Tensile toughness (J cm^{-3})
EVA	8.95 ± 0.18	5.62 ± 0.29	1470.55 ± 13.00	71.15 ± 1.20
Self-cross-linked TMS-PE	14.22 ± 1.10	115.29 ± 3.66	349.56 ± 41.04	44.04 ± 1.54
Si60	14.14 ± 0.14	24.13 ± 1.73	899.38 ± 20.54	70.51 ± 2.36
Si90	15.87 ± 0.52	38.19 ± 1.02	804.77 ± 9.62	76.98 ± 3.66
Si90$_{1st}$	13.48 ± 1.03	35.11 ± 1.50	756.36 ± 31.25	75.49 ± 2.57
Si90$_{2nd}$	14.27 ± 0.35	39.98 ± 0.72	799.84 ± 17.72	78.56 ± 2.66
Si120	16.29 ± 0.54	50.41 ± 2.34	665.64 ± 14.01	68.58 ± 4.44

Moreover, the tensile toughness of Si90 remained almost unchanged after three cycles of reprocessing.

4. Conclusion

In conclusion, we propose a strategy for constructing PE vitrimers *via* direct cross-linking of two mass-produced ethylene-based polymers. Through a one-step reactive blending approach, PE vitrimers with dynamic Si–O–C cross-linkages were successfully prepared *via* the transesterification between silicate in TMS-PE and carboxylate in EVA. The observed torque increase during reactive blending, attributed to cross-linking-induced viscosity rise, served as direct evidence for the successful synthesis of PE vitrimers. FTIR analysis revealed the consumption of ester groups in the EVA, thereby confirming the occurrence of the transesterification. Furthermore, gel fraction testing offered strong evidence for the formation of a robust cross-linked network. The resulting PE vitrimers exhibited clear rubbery plateaus and excellent high-temperature creep resistances, underscoring the role of Si–O–C cross-linkages in enhancing the stability of the vitrimer network. The E_a of the Si–O–C bonds was determined to be 74.5 kJ mol^{-1}, which is close to the reported values for Si–O–C based polyolefin vitrimers. Compared to virgin EVA, the tensile strength of PE vitrimers almost doubled while the Young's modulus grew eightfold. Moreover, the incorporation of dynamic covalent bonds enables excellent reprocessability, with tensile

strength, Young's modulus, and elongation at break remaining almost unchanged after reprocessing two times. The PE vitrimers developed in this study offer significant advantages in terms of ease of processing, low cost, and high performance, highlighting their strong potential for a wide range of applications.

Author contributions

Y. Zhang and X. Li conceived the study and designed the experiments. X. Zhang performed most of the experiments. Y. Zhang and X. Zhang wrote the manuscript. X. Li contributed to the discussion of results and language editing. S. Guo helped in discussing the results and polishing the language. All authors reviewed and approved the final manuscript.

Conflicts of interest

A provisional patent application has been filed on the process and composition of the resulting materials with Y. Z., X. Z, X. L., and S. G. as inventors.

Data availability

The authors declare that the data supporting the findings of this study are available within the paper and its supplementary information (SI). The Supplementary Information includes tables (gel fraction and ester conversion data, thermal properties data, storage modulus and molecular weight between cross-links data, mechanical property comparison data for commercial vinyl polymers, and ester conversion data for Si90 before and after crosslinking), figures (SEM images and silicon element distribution maps of PE vitrimers, TGA curves, a fitted curve of initial decomposition temperature *versus* TMS-PE content, creep curves, and FTIR curves), and equations (calculation formulas for ester conversion and molecular weight between cross-links). See DOI: https://doi.org/10.1039/d5lp00399g.

Should any raw data files be needed in another format, they are available from the corresponding author upon reasonable request.

Acknowledgements

The authors thank the financial supports from the Department of Education of Liaoning Province (Grant No. LJ212510152025) and the National Natural Science Foundation of China (Grant No. 22404013).

References

1 J. Thomas, B. Joseph, J. P. Jose, H. J. Maria, P. Main, A. Ali Rahman, B. Francis, Z. Ahmad and S. Thomas, *Ind. Eng. Chem. Res.*, 2019, **58**, 20863–20879.
2 K. Aljoumaa and A. W. Allaf, in *Crosslinkable Polyethylene: Manufacture, Properties, Recycling, and Applications*, ed. J. Thomas, S. Thomas and Z. Ahmad, Springer Singapore, Singapore, 2021, pp. 125–166, DOI: 10.1007/978-981-16-0514-7_6.
3 A. J. Shapiro, P. J. Brigandi, M. Moubarak, S. S. Sengupta and T. H. Epps, III, *ACS Appl. Polym. Mater.*, 2024, **6**, 11859–11876.
4 C. Blivet, J.-F. Larché, Y. Israëli and P.-O. Bussière, *Polym. Degrad. Stab.*, 2022, **201**, 109978.
5 C. Li, C. Zhang, H. Zhao, H. Zhang, X. Wang and B. Han, *Polym. Degrad. Stab.*, 2021, **185**, 109498.
6 M. G. Andersson, M. Jarvid, A. Johansson, S. Gubanski, M. R. S. Foreman, C. Müller and M. R. Andersson, *Eur. Polym. J.*, 2015, **64**, 101–107.
7 V. V. Tcherdyntsev, S. D. Kaloshkin, A. A. Lunkova, A. M. Musalitin, V. D. Danilov, Y. V. Borisova, A. A. Boykov and V. A. Sudarchikov, *J. Alloys Compd.*, 2014, **586**, S443–S445.
8 N. Mostofi Sarkari, M. Mohseni and M. Ebrahimi, *J. Appl. Polym. Sci.*, 2019, **136**, 47147.
9 A. A. Yussuf, M. A. Al-Saleh, S. T. Al-Enezi and G. Abraham, *Polym. Compos.*, 2021, **42**, 2268–2281.
10 J. M. Garcia and M. L. Robertson, *Science*, 2017, **358**, 870–872.
11 K. Liu, Y. Zhao, A. M. Wolff, K. L. Harry, E. M. Rettner, J. Miscall, N. A. Rorrer and G. M. Miyake, *Angew. Chem., Int. Ed.*, 2025, **64**, e202502641.
12 A. E. Gerdroodbar, V. Karimkhani, E. Dashtimoghadam and M. Salami-Kalajahi, *J. Environ. Chem. Eng.*, 2024, **12**, 112897.
13 Q. Shi, C. Jin, Z. Chen, L. An and T. Wang, *Adv. Funct. Mater.*, 2023, **33**, 2300288.
14 J. Luo, Z. Demchuk, X. Zhao, T. Saito, M. Tian, A. P. Sokolov and P.-F. Cao, *Matter*, 2022, **5**, 1391–1422.
15 D. Montarnal, M. Capelot, F. Tournilhac and L. Leibler, *Science*, 2011, **334**, 965–968.
16 M. Ahmadi, A. Hanifpour, S. Ghiassinejad and E. van Ruymbeke, *Chem. Mater.*, 2022, **34**, 10249–10271.
17 E. Albertini, S. Dalle Vacche and A. Vitale, *RSC Appl. Polym.*, 2026, DOI: 10.1039/D5LP00408J.
18 G. Ye, S. Huo, C. Wang, Q. Zhang, H. Wang, P. Song and Z. Liu, *Small*, 2024, **20**, 2404634.
19 H. Liu, X. Liu, L. Wang, B. Zeng, Q. Zhao, W. Luo, Y. Xu, C. Yuan and L. Dai, *Composites, Part B*, 2025, **297**, 112316.
20 D. Liu, Y. Xiao, W.-C. Nie, L.-Y. Shi, C.-J. Fan, K.-K. Yang and Y.-Z. Wang, *Composites, Part A*, 2025, **190**, 108624.
21 B. Hendriks, J. Waelkens, J. M. Winne and F. E. Du Prez, *ACS Macro Lett.*, 2017, **6**, 930–934.

22 M. M. Obadia, B. P. Mudraboyina, A. Serghei, D. Montarnal and E. Drockenmuller, *J. Am. Chem. Soc.*, 2015, **137**, 6078–6083.
23 H. Gao, Q. Zhao, L. Xu, Z. Wang, B. Wang, D. Wang, L. Jin and Y. Xia, *Macromolecules*, 2025, **58**, 1705–1716.
24 C. Bodhak, P. Sahu and R. K. Gupta, *Polymer*, 2025, **320**, 128095.
25 M. Xiang, F. Dong, Y. Guo, X. Li, J. Chen, H. Wang, Y. Chen, Y. Liu and A. Du, *J. Colloid Interface Sci.*, 2025, **693**, 137568.
26 K. Dong, D. Zhao, Y. Pang, B. Liu, Q. Liu, T. Mu and C. Zhao, *Chem. Eng. J.*, 2025, **508**, 160754.
27 F. Wang, X. Lu and Z. Xin, *Prog. Org. Coat.*, 2025, **203**, 109168.
28 B. Shan, X. Cao, Z. Hao, K. Wei and B. Tang, *Constr. Build. Mater.*, 2025, **463**, 140053.
29 X. Wen, C. Hong, H. Li, F. Xu, Y. Li and J. Sun, *Nano Energy*, 2024, **125**, 109561.
30 R. Górecki, S. Bhaumik, E. Qasem, L. Loiola, A.-H. Emwas, K. Ntetsikas, N. Hadjichristidis and S. P. Nunes, *Small*, 2025, **21**, 2409139.
31 L.-Y. Li, W. Chen, C.-H. Hu, Y.-D. Li and J.-B. Zeng, *ACS Sustainable Chem. Eng.*, 2025, **13**, 547–558.
32 Y.-W. Huang, M. J. Suazo and J. M. Torkelson, *Macromolecules*, 2025, **58**, 4847–4859.
33 Z. Wang, Y. Liu, W. Pang, A. Chen and M. Chen, *Sci. China: Chem.*, 2024, **67**, 3861–3867.
34 S. Bhaumik, G. Zapsas, A. A. Farah, H. Bouchekif, N. Verghese and N. Hadjichristidis, *Eur. Polym. J.*, 2025, **233**, 113960.
35 B. Wang, Y.-C. Gao, H. Wang and H. Niu, *Chin. J. Polym. Sci.*, 2024, **42**, 1557–1565.
36 R. B. da Cunha, L. B. Q. Brito, P. Agrawal, G. d. F. Brito and T. J. A. d. Mélo, *Macromolecules*, 2024, **57**, 7953–7969.
37 I. Dey, K. Samanta, S. Ghosh, T. Debnath, S. Mandal, S. S. Rege, S. Vimal Kumar, S. Safikul Islam, A. Misra and S. Bose, *Chem. Eng. J.*, 2025, **504**, 158696.
38 I. Dey, D. Kundu, S. Ghosh, S. Mandal, K. Samanta and S. Bose, *Nanoscale Adv.*, 2025, **7**, 2904–2915.
39 S. Wang, S. Gao, X. Zhang, X. Li and Y. Zhang, *J. Polym. Environ.*, 2025, **33**, 1445–1458.
40 L. Cheng, S. Liu and W. Yu, *Polymer*, 2021, **222**, 123662.
41 S. Lai, Q. Tan, H. Xie, J. Gong, L. Xue, H. Liu, R. Zhang, Y. Li and S. Bai, *RSC Appl. Polym.*, 2025, **3**, 1216–1229.
42 Y. Ouyang, M. Mauri, A. M. Pourrahimi, I. Östergren, A. Lund, T. Gkourmpis, O. Prieto, X. Xu, P.-O. Hagstrand and C. Müller, *ACS Appl. Polym. Mater.*, 2020, **2**, 2389–2396.
43 Z. Li, Y. Wen, Z. Song, C. Zhang, C. Cui, D. An, Z. Ge, Y. Cheng, Q. Zhang and Y. Zhang, *ACS Macro Lett.*, 2023, **12**, 1409–1415.
44 Z. Zhang, K. Wu, H. Sui, G. Zhao, Y. Wu, C. Cui, P. Zhao, K. Yang, L. Zhong, B. Wan, S. Li, Z.-M. Dang and J. Li, *Chem. Eng. J.*, 2025, **521**, 166714.
45 H. Guo, L. Yue, G. Rui and I. Manas-Zloczower, *Macromolecules*, 2020, **53**, 458–464.
46 C. A. Tretbar, J. A. Neal and Z. Guan, *J. Am. Chem. Soc.*, 2019, **141**, 16595–16599.
47 J. Zhang, X. Li, S. Zhang, W. Zhu, S. Li, Y. Zhang, Y. Hu and G. Zhou, *ACS Appl. Polym. Mater.*, 2023, **5**, 8379–8386.
48 S. S. Sengupta, in *Crosslinkable Polyethylene: Manufacture, Properties, Recycling, and Applications*, ed. J. Thomas, S. Thomas and Z. Ahmad, Springer Singapore, Singapore, 2021, pp. 41–66, DOI: 10.1007/978-981-16-0514-7_3.
49 H. Gao, Y. Gao, J. Zhang, J. Wang, Y. Yang, W. Wang and Y. Cao, *Polymer*, 2025, **323**, 128168.
50 M. Faker, M. K. Razavi Aghjeh, M. Ghaffari and S. A. Seyyedi, *Eur. Polym. J.*, 2008, **44**, 1834–1842.
51 Y. Zhang, X. Li, W. Wang, S. Wang, J. Xu, L. Xu and H. Li, *React. Funct. Polym.*, 2018, **122**, 68–74.
52 M. Fan, Y. Zhang, X. Li, B. Zeng, S. Chen, W. Zhu, S. Wang, J. Xu and N. Feng, *Polym. Adv. Technol.*, 2019, **30**, 1226–1233.
53 M. Kränzlein, S. Cui, J. Hu, A. M. LaPointe, B. P. Fors and G. W. Coates, *J. Am. Chem. Soc.*, 2025, **147**, 19052–19060.
54 S. Zheng, S. Zhong, X. Liu and S. Sun, *Chem. Eng. J.*, 2025, **509**, 161485.
55 Z. Qin, Y. Li, H. Huang, Y. Wang, Z. Wang, F. Tian, J. Jiang and W. Zhai, *Sustainable Mater. Technol.*, 2025, **45**, e01583.
56 S. Guo, X. Zhang, X. Li and Y. Zhang, *ACS Appl. Polym. Mater.*, 2025, **7**, 14392–14400.
57 H. Ramli, N. F. A. Zainal, M. Hess and C. H. Chan, *Chemistry Teacher International*, 2022, **4**, 307–326.
58 J.-P. Queslel and J. E. Mark, in *Encyclopedia of Physical Science and Technology (Third Edition)*, ed. R. A. Meyers, Academic Press, New York, 2003, pp. 813–839, DOI: 10.1016/B0-12-227410-5/00198-8.
59 B. Soman and C. M. Evans, *Soft Matter*, 2021, **17**, 3569–3577.
60 Y. Du and D. Wang, *ACS Appl. Mater. Interfaces*, 2024, **16**, 41551–41561.
61 M. Fang, X. Liu, Y. Feng, M. Huang, C. Liu and C. Shen, *Compos. Sci. Technol.*, 2024, **255**, 110731.
62 Y. Kohsaka, M. Mizuma and M. Hayashi, *RSC Appl. Polym.*, 2026, **4**, 211–217.
63 A. Jamei Oskouei, E. Mao, T. G. Gray, A. Bandegi, S. Mitchell, M. K. Sing, J. Kennedy, K. Miller McLoughlin and I. Manas-Zloczower, *RSC Appl. Polym.*, 2024, **2**, 905–913.
64 N. Nishiie, R. Kawatani, S. Tezuka, M. Mizuma, M. Hayashi and Y. Kohsaka, *Nat. Commun.*, 2024, **15**, 8657.
65 Y. Shan, F. Dong, Y. Feng, Z. Nie, H. Xu, R. Wang and S. Qi, *Eur. Polym. J.*, 2025, **236**, 114143.
66 M. Capelot, M. M. Unterlass, F. Tournilhac and L. Leibler, *ACS Macro Lett.*, 2012, **1**, 789–792.
67 S. Tripathi, H. Supriya and S. Bose, *SPE Polym.*, 2024, **5**, 136–150.
68 W. Denissen, J. M. Winne and F. E. Du Prez, *Chem. Sci.*, 2016, **7**, 30–38.
69 Q. Li, D. Wang, T. Wang, Y. Zhang, S. Liu, S. Zhang, Z. Hu, L. Li, G. Wang and Y. Zhao, *RSC Appl. Polym.*, 2025, **3**, 1183–1192.

70 Y. Nishimura, J. Chung, H. Muradyan and Z. Guan, *J. Am. Chem. Soc.*, 2017, **139**, 14881–14884.
71 B. Zhao, G. Hang, L. Li and S. Zheng, *Mater. Today Chem.*, 2022, **24**, 100759.
72 Z. Wang, Y. Gu, M. Ma, Y. Liu and M. Chen, *Macromolecules*, 2021, **54**, 1760–1766.
73 X. Zuo, B. Wang, O. Ejeromedoghene, S. Ye and G. Fu, *J. Mol. Struct.*, 2023, **1294**, 136305.